

escopes. An article by Selman et al. describes the development of this software and how it was put in place over the existing control software.

Recent work by J. Manfroid and F. Selman has demonstrated that the amplitude of the flat-field calibration error plays a significant role in photometric accuracy with the WFI at the level of a few per cent. The accompanying article by Manfroid, Selman & Jones describes a dithering technique that allows observers to correct for this, with examples demonstrating its effect on some photometry. Any observers requiring WFI photometry to better than a few per cent are encouraged to look into this procedure.

### Multi-Object Spectroscopy at the Danish 1.54-m

Multi-Object Spectroscopy (MOS) was recently performed successfully with DFOSC at the Danish 1.54-m tele-

scope. The observational procedure requires one to take a pre-image of the required field(s), send the image files to Copenhagen (where a punching machine creates the mask), and finally to ship the mask(s) back to La Silla in time for the spectroscopic observations. The mask is placed in the DFOSC slit wheel and aligned on the sky using a MIDAS procedure (kindly made available by P. Leisy of the NTT Team and modified for use at the Danish 1.54 by E. Pompei). The procedure calculates the offsets between the object centres and those of the corresponding slitlets, correcting for the alignment by applying a fine rotation to the DFOSC slits wheel.

To make this possible, it is necessary to bypass the DAISY acquisition system, through a C-shell script that accepts direct input from the instrument workstation to the PC controlling DFOSC. The new mode was tested during February 2001 in Danish time,

with Prof. L. Hansen (Niels Bohr Institute, Copenhagen University). Long slit spectra of galaxies in the EIS field 61 were successfully acquired: Figure 1 is a 20-min exposure of a field full of spectra. A new flat-field lamp will soon be installed in the sky baffle, to allow the acquisition of flats without the need to change telescope position, hopefully expediting calibration.

The effectiveness of this system will be checked when it is installed. The final implementation was the result of interaction between the Copenhagen University (in particular Per Kjaergaard Rasmussen, Michael I. Andersen, Morten Liborius Jensen and Anton Norup Soerensen) and the 2p2 Team.

The MOS mode has been offered since the beginning of March this year but is only available in Danish Time (not ESO Time). Any observer wishing to use it must include the time for pre-imaging time in the estimate of the total time requirements.

## Commissioning the Spectroscopic Mode of the WFI at the MPG/ESO 2.2-m Telescope at La Silla

L. WISOTZKI<sup>1</sup>, F. SELMAN<sup>2</sup>, A. GILLIOTTE<sup>2</sup>

<sup>1</sup>Universität Potsdam, Germany, lutz@astro.physik.uni-potsdam.de

<sup>2</sup>La Silla Observatory, European Southern Observatory, Chile, fselman@eso.org, agilliot@eso.org

### 1. Introduction

For Period 68, the Wide Field Imager at the MPG/ESO 2.2-m telescope at La Silla will offer, in addition to the imaging mode, a spectroscopic mode. This will be accomplished by the installation of a grism in front of the WFI triplets to allow for slitless spectroscopy. The combination of the wide field of view, the grism, and the simultaneous availability of the whole set of WFI filters, make this a unique instrument in the southern skies. The instrument will be operated in VLT mode, with the instrument package with the spectroscopic templates already released.

In a preliminary ESO internal report by Hermann Boehnhardt, now at Paranal, the following case was made for the spectroscopic mode of the WFI. This mode will allow survey work for stellar, nebular objects, and galaxies with special characteristics. The main goal would be the registration and identification of such sources by their spectral signatures to establish population and distribution statistics and to prepare in-depth follow-up investigations by dedicated research programmes with other telescopes and instruments.

A rough estimate of the gain in sensitivity for the WFI at the MPG/ESO

2.2-m telescope as compared to objective prism spectroscopy at Schmidt telescopes gives: gain in aperture by a factor of 4–5, gain by CCD sensitivity as opposed to photographic emulsion

by a further factor of 20 or more, for a total factor of 100 in sensitivity gain. The advantage of the WFI in spectroscopic mode with respect to standard CCD spectrographs at 2–4-m-class tel-

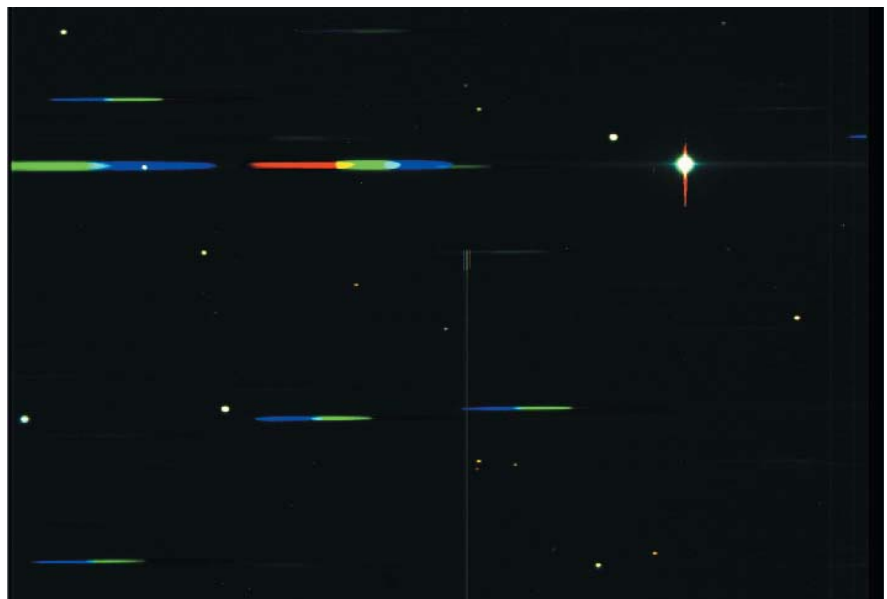


Figure 1: Portion of chip 51 showing the spectra of several stars taken using the WFI and grism B50. Notice the large amount of flux going into the 0th and negative orders. Also notice the white, 0th order image on top of one of the spectra; from its colour it is obvious that this is not an emission feature.

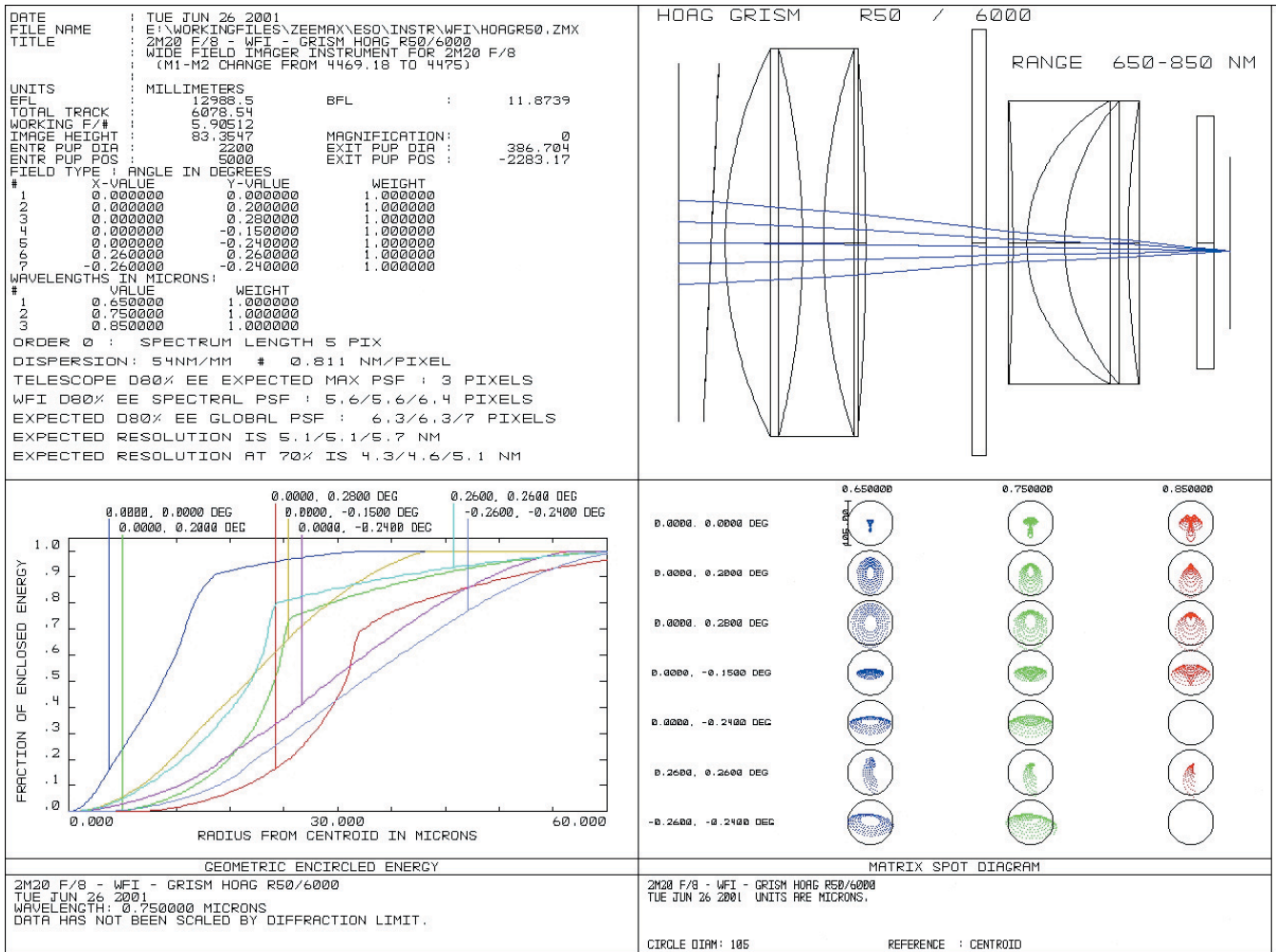


Figure 2: Optical simulation of the WFI with the R50 grism. First quadrant: optical data such as field sizes, wavelengths and resolutions. Second quadrant: layout of the WFI; the light comes from the left and the filter (thin large rectangle) is between the two lens triplets in a converging  $f/5.9$  beam. Third quadrant: encircled energy of the telescope/WFI. Fourth quadrant: spot diagrams at different points (X, Y) in the field.

scopes is its much larger field of view, and its ability to obtain spectra of all objects therein at once.

In the preliminary draft mentioned above, the following areas of research were identified:

- search for stars with emission lines,
- search for stars with peculiar molecular lines,
- search for white dwarfs,
- detection of stars with strong magnetic fields,
- detection of  $H\alpha$  emission-line stars in dark clouds,
- search for Herbig-Haro objects,
- search for stars at large distances above the galactic disk,
- detection of extragalactic HII regions and planetary nebula,
- detection of objects without obvious spectral lines,
- membership in distant galaxy clusters,
- search for emission-line galaxies and quasars,
- detection of galaxies with peculiar continuum at high redshift,
- search for lensed quasars.

The potentialities of the instrument can be gauged by looking at the survey results by Schneider, Schmidt, and

Gunn (1994). These authors, using the 4-shooter in scanning mode at the Hale 5-m telescope at Palomar Mountain, covered a 61-degree area of the sky with an effective exposure time per strip ranging from 34s to 63s (the WFI in 10 hours integration covers an equivalent volume): they obtained spectra for 600,000 objects, with approximately 800 emission-line galaxies, and 90 quasars. The same authors in a deeper survey, with 300 s effective exposure time, and 1.10 square degrees effective area, find approximately 50 low-redshift emission-line galaxies, 9 high-redshift  $z > 2.7$  quasars (Schneider, Schmidt, and Gunn 1999).

Here we describe the instrument configuration for spectroscopic observations, and summarise the results of two commissioning runs done during March 2001.

Table 1: Summary of properties of the WFI grisms.

Grism	Blaze wavelength nm	Wavelength Range		Dispersion		IQ Resolution	
		nominal nm	measured nm	nominal nm/pix	measured nm/pix	pix	nm
B50	400	400–650	380–740	0.807	0.701	4.5	3.1
R50	600	650–850	420–900	0.811	0.691	6.3	4.4

## 2. Image Quality and Calibration

In Table 1 we present a summary of simulated and measured properties of the two available grisms. The wavelength range has been defined as that portion over which the efficiency is above 25% of the measured peak efficiency, and has been read directly from the measured response curves for the B50 and R50 grisms. As we discuss below, the B50 grism is so much inferior compared to the R50, even in the blue, that we will concentrate the discussion on the red grism.

### 2.1 Simulated Optical Properties

Because of the geometry of the WFI instrument, the dispersing elements have to be placed in the converging

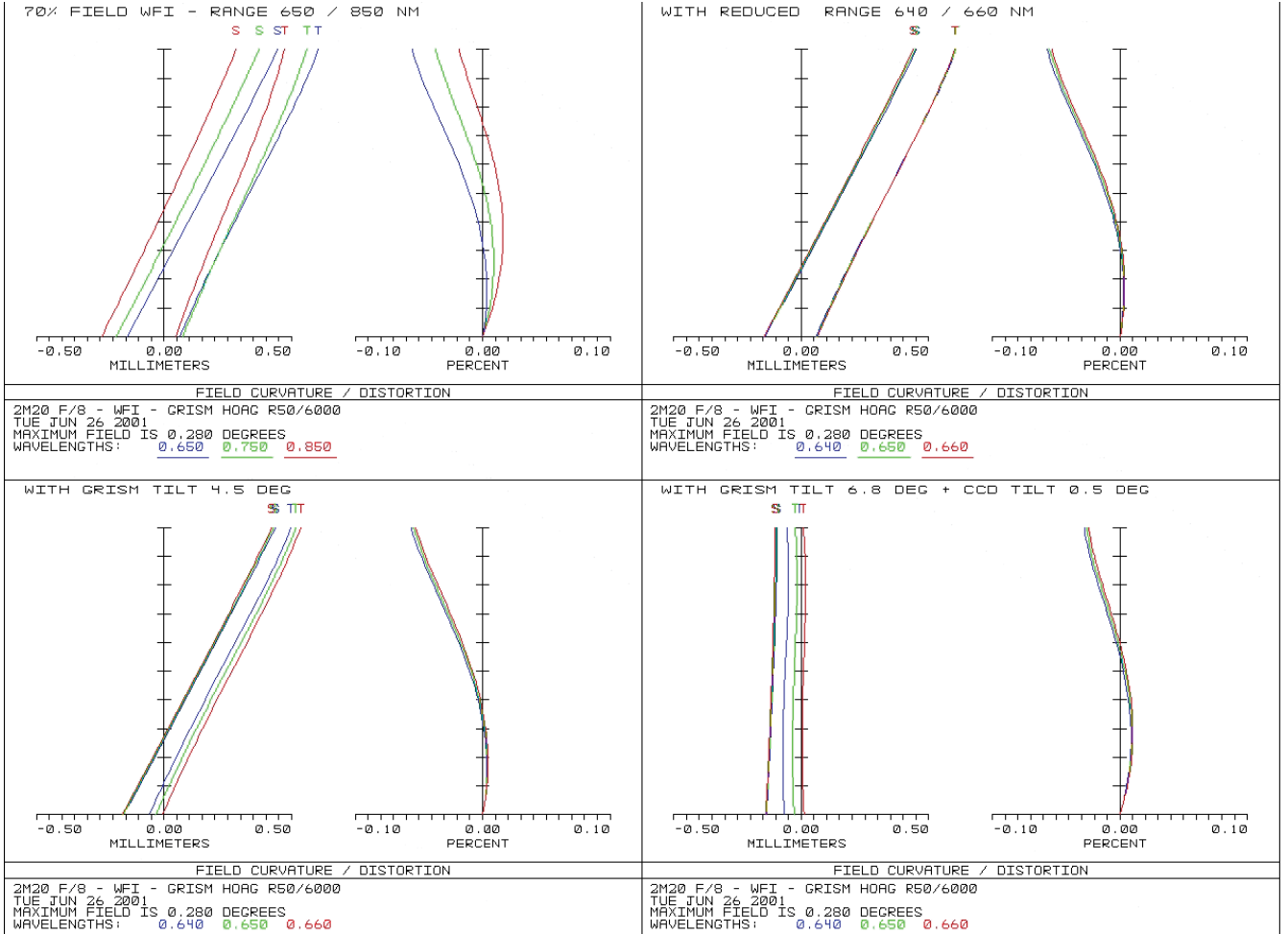


Figure 3: Optical simulation of the field curvature and distortion for several configurations of the WFI + R50 grism. Top left, full wavelength range, and top right, restricted wavelength range centred at  $H\alpha$ . Bottom panels: restricted wavelength range centred at  $H\alpha$  with left, tilted grism, and right, tilted grism + tilted CCD, a combination which minimises the defocus.

beam where they induce larger aberrations (see the classical papers by Hoag and Schroeder 1970 and by Bowen and Vaughan 1973). Thus, a careful optical analysis had to be conducted.

A technical/feasibility study was performed by one of the authors in 1998 (*WFI Grism Spectroscopy*, LSO-TREESO-75441-001, Gilliotte 1998). It contains simulations of the optical properties expected with the different available grisms. Because of its superior efficiency and order rejection properties, we concentrate below in a description of the R50 grism.

#### R50/6000 Grism

The dispersion of this grism was calculated to be 54 nm/mm, or 0.811 nm/pixel. The geometric encircled energy plots show a predicted 80% monochromatic imaging quality of 5.6, 5.6 and 6.4 pixels, for each wavelength, to be convolved with an assumed telescope PSF of 3 pixels. The global image quality will amount to 6.3, 6.3, and 7.0 pixels respectively when the external seeing is 0.65 arcsec. The nominal spectral resolution is then around 5.1, 5.1, and 5.7 nm for  $\lambda = 650$  nm, 750 nm, and 850 nm, respectively (in general,

the resolution in slitless spectroscopy depends on the seeing and will be degraded in case of poor seeing conditions). Notice that the actually measured dispersion is slightly lower than the nominal value.

Technical data:

- corning B1664 prism of 2.49 degrees
- replica 53.33 gr/mm with 3.42 blaze angle
- triplet properties: 54 nm/mm with blaze wavelength at 590 nm

Figures 2 and 3 show the field curvature, distortion, and the spot diagram plots obtained under the following four instrumental set-ups: (1) 70% of the full field; (2) after reducing the wavelength range around  $H\alpha$ ; (3) after tilting the grism alone; and (4) after both grism

and CCD tilt. Grism tilt reduces longitudinal astigmatism by a factor of 1.5, but final image quality does not improve much (coma). Only CCD tilt improves the image quality drastically, with image below 2 pixels, meaning 2.9 nm over the full field. However, as of this writing there are no plans to offer a set-up with a tilted CCD for Period 68.

#### 2.2 Measured optical properties

The simulations described in the previous section established that the best image quality of the R50 grism can be obtained with a tilt of the grism itself and also of the CCD. Because we did not tilt the CCD, we thought it important to perform actual measurements regarding the degradation of image quality.

Table 2: Efficiencies of the WFI + grisms (counts in first order).

Filter	ETC counts $e^-$	B50 counts $e^-$	R50 counts $e^-$
U 350	19	12	
B	222	81	108
V	248	68	150
R	543	111	429
I	371		176
White	1729	387	$\approx 1100$

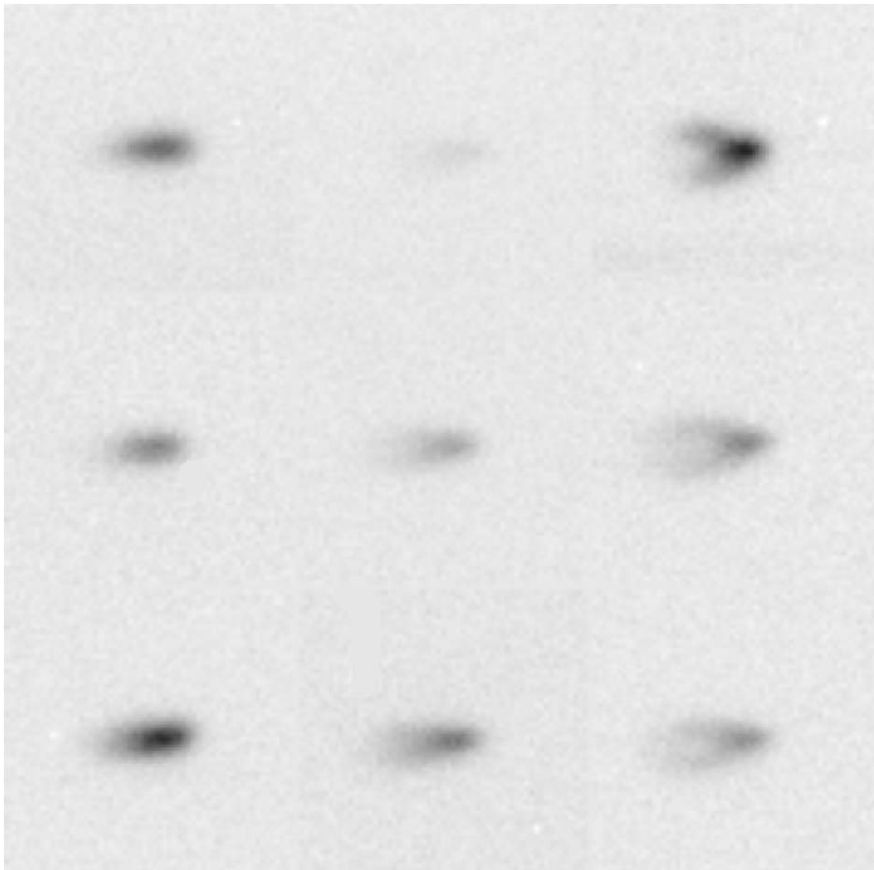


Figure 4: Shape of the zeroth orders in different parts of the mosaic as measured with the R50 grism and the B filter. The scale is such that the vertical and horizontal distances between images correspond to 60 pixels or 14 arcsec.

Figure 4 shows the image quality with the R50 grism together with the B filter. Although what we show is the shape of the 0th order, and not that of an emission-line feature in the first order, we can see that the simulations did a good job at predicting the effect. The nine images are extractions of 0th orders in different parts of the mosaic: the top row shows images extracted in the upper parts of chip 51, 52, and 53; the middle row shows images extracted at the bottom of the same chips; and the bottom row shows images extracted at the bottom of chips 56, 55, and 54.

Figure 5 shows a better example of the achievable quality. It shows extracts from a 900 s image through the R50 grism and the medium-band filter MB516. The arrangement in the montage is as before. The numbers are the FWHM of the vertical distribution of light at the centre of each spectra, measured in pixels (1 arcsec = 4.2 pix).

Another important property is the ability to superimpose dithered images. What we did was to use the astrometry tasks of the IRAF astrometry package, mscred, to superimpose the zeroth orders, and then see how well the first orders matched. We produced an animation that you can see in the web version of this document, at <http://www.lis.eso.org/lasilla/Telescopes/2p2T/E2p2M/WFI/grism>.

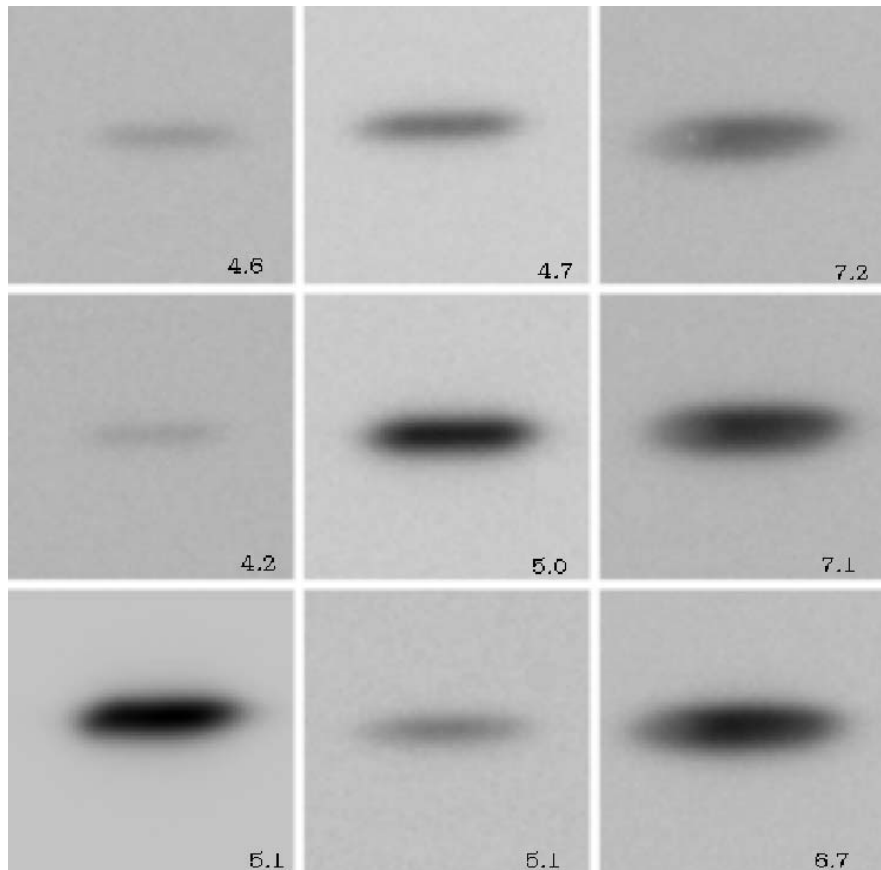


Figure 5: Shape of the first order as measured with the R50 grism and the MB516 filter. Scale set in same way as in previous figure.

The animation shows a portion of three dithered images centred on a bright quasar. One can see that the emission lines superimpose rather well.

### 2.3 Flux calibration and efficiencies

Table 2 summarises the data on the overall response of the telescope plus grism plus WFI. The numbers reported are the integrals over the response curves. They assume a source having a flat spectrum with  $f_{\lambda} = \text{const.} = 1 \times 10^{-16} \text{ erg s}^{-1} \text{ cm}^{-2} \text{ \AA}^{-1}$  (corresponding to a Vega magnitude of  $V = 18.83$ ), observed with an exposure time of 1 s. For comparison, we list also the count rates estimated by the WFI exposure time calculator for direct imaging in each filter; the ratio between these and the grism counts gives directly the efficiency losses due to the grism.

Figures 6 and 7 show the response curves of the two grisms obtained by observing the HST flux standard GD108. The units of the ordinates are electrons/pixels/seconds. Notice that even in the blue the R50 grism has a much higher response than the B50. The main reason for this unexpected behaviour are the substantial flux losses to other than the first spectral order in the B50 grism, discussed in more detail below.

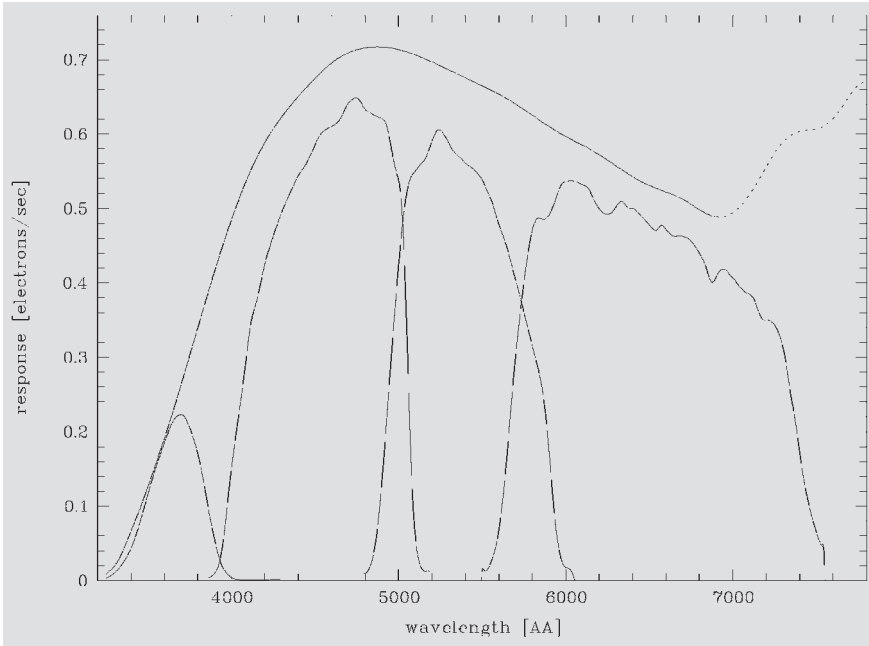


Figure 6: Response curves for the B50 grism with no filter, and with the U 350, B, V, and R filters.

Notice that above 690 nm for the B50, and 640 for the R50, the curves for no filter (“white”) are heavily contaminated with light from the second order (dotted lines). As soon as filters are used, no such contamination occurs since the orders will always be spatially well separated.

#### Diffusion of flux into adjacent orders

Table 3 shows the relative flux distribution among the different orders. The 1st order has always been set to 100. The R50 grism has a much better characteristic than the B50: while the latter allows more than 50 % of the flux to spill over into unwanted orders, the former concentrates more than 90% of the flux in the first order (in the *R* band). This results in an almost total lack of 0th-order images when observing with some red medium-band filters, a fact that could somewhat complicate the wavelength calibration (but see our suggestions below on observing strategies). Indeed, the better suppression of unwanted orders by the R50 makes it outperform the B50 even in the *B* band, despite the latter’s nominal “blue” classification.

#### 2.4 Wavelength calibration

Table 4 summarises the measured dispersions of the two available grisms. The wavelength calibrators used were the Seyfert 1 galaxy Mrk 1239, which shows several emission lines over the entire spectral range, and a number of M-type stars with prominent TiO absorption bands. The object was placed near the centre of the array, and in several positions near the corners and edges. In the absence of accompany-

ing direct images, the 0th order centroids were used to define the wavelength zero points. We found that the true zero points varied substantially, up to  $\sim 3$  pixels between different locations on the array in a nontrivial manner, probably as a result of optical distortions induced by the grism. Unless a much more detailed investigation shows how to model these distortions, this effect ultimately limits the achievable wavelength calibration accuracy to  $\sim \pm 15$  Å or so.

The dispersion relations of both grisms are well described by 2nd-order polynomials (see Fig. 8). Given the

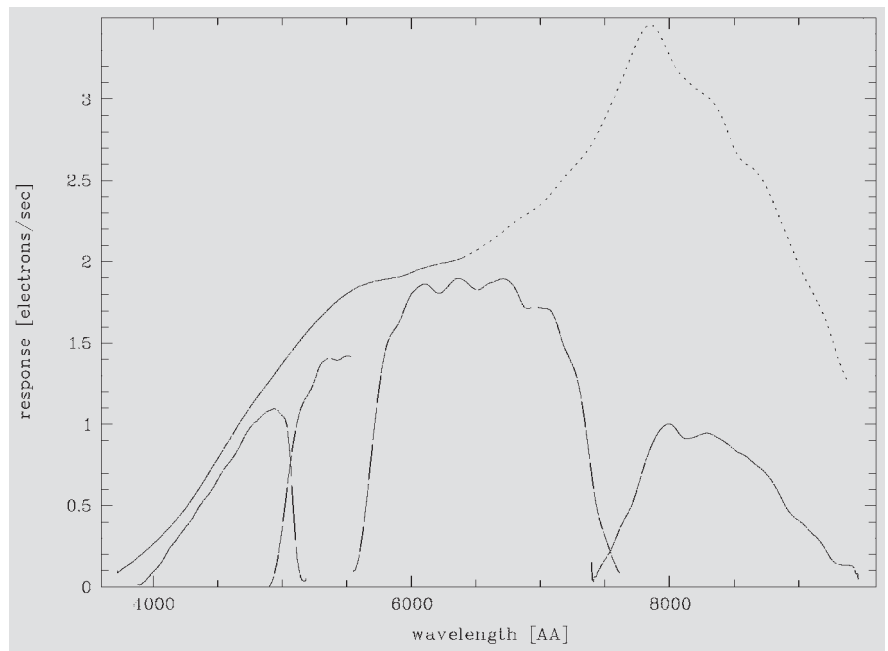


Figure 7: Response curves for the R50 grism with no filter, and with the B, V, R, and I filters. Notice the different scale between this graph and that of the B50 grism: the R50 grism is better than the B50 even in the blue.

Table 3: Distribution of flux among orders.

Order	Grism B50 B	Grism R50 B	R
-4	3		
-3	6	0.1	
-2	9	0.4	0.8
-1	16	2	1.6
0	42	7	2.3
+1	100	100	100
+2	4	29	0.4
+3	1	2	
+4		0.4	
+5		0.1	

substantial zero point uncertainties, in most practical cases it is probably sufficient to work with a linear dispersion relation, as the maximum systematic error will be substantially less than the zero-point variations except for white light (no filter) images, which we strongly discourage anyway.

### 3. Observing

#### 3.1 Example spectra

We present in this section a few real extracted and calibrated spectra so that future users obtain a better idea of the capabilities of the instrument.

#### Flux standard star

Figure 9 shows the HST flux standard GD 108, a hot subdwarf with distinct Balmer absorption lines, observed with the WFI R50 grism and the *B*, *R*, and *I* broad-band filters. Integration time for each of these exposures was 100 sec.

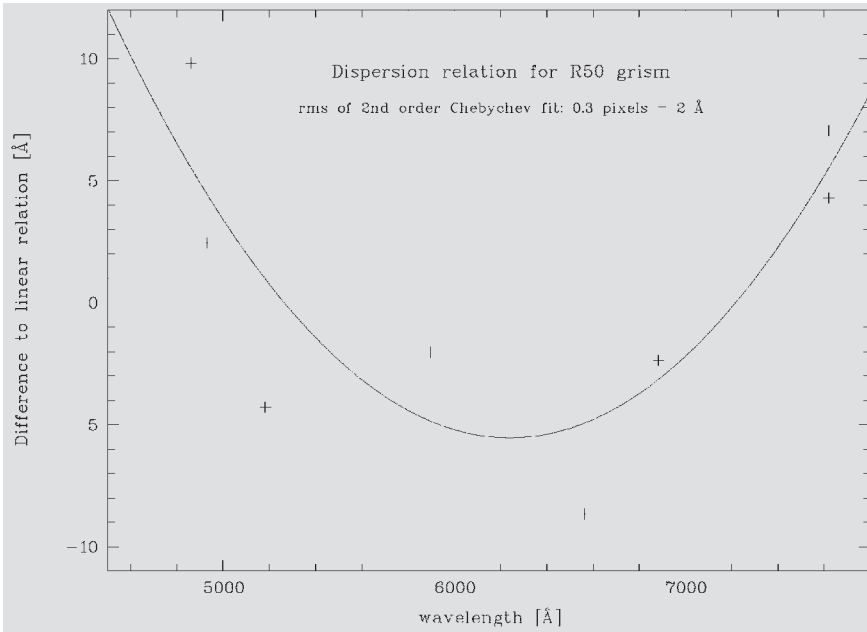


Figure 8: Quadratic dispersion solution for the R50 grism.

Table 4: Global dispersions of the WFI grisms.

Grism	Measured Dispersion nm/pix	Spatial Variation	
		%	pix
B50	0.701	1	2–3
R50	0.691		N/A

Slitless spectroscopy has one rather obvious property which is nevertheless worth recalling: Slit losses are naturally avoided as there is no slit, and the extracted spectra are therefore easily placed onto a proper (at least relative) flux scale.

#### Comparison between a slitless and a slit spectrum

Figure 10 shows the extracted slitless spectrum of our wavelength calibrator, the Seyfert galaxy Mrk 1239 (plotted in black), obtained with the B50 grism in white light. This is contrasted with a slit spectrum of the same object taken in 1997 with the ESO 1.52-m telescope and the Boller&Chivens spectrograph (upper spectrum plotted in red). The original B&C spectrum has somewhat better spectral resolution, and we therefore smoothed it to approximately the same resolution as the WFI spectrum. The resemblance of the two datasets is striking and illustrates the fidelity by which spectral information can be extracted from WFI slitless spectroscopy.

### 3.2 Hints for observing

The Wide Field Imager in its slitless spectroscopic mode is a powerful and almost unique instrument to conduct surveys for objects with characteristic spectral signatures. This final section

is meant to help interested potential users planning such a survey, and to provide some guidelines for data reduction.

#### Always observe with a filter

Without filter, there are several substantial drawbacks that will severely reduce the usefulness of your data:

The background would be prohibitively high for deep surveys as all the sky contributions over the entire spectral range go into each pixel.

2. The spectra are much longer, and the losses because of overlapping spectra will be substantially increased.

3. Contamination by 2nd-order spectra limit the exploitable spectral range to below ~ 650 nm.

#### Always obtain a direct image of your field

Although it is technically possible, in principle, to use the 0th orders to define objects and determine wavelength calibration zero points, we *strongly* recommend to use paired direct images for this purpose. This recommendation is based on the experience collected in the course of the Hamburg/ESO survey, a large quasar survey based on digitised objective-prism Schmidt plates (Wisotzki et al. 2000; see also Reimers & Wisotzki 1997). These papers also outline a working strategy for object definition, extraction and wavelength calibration for slitless spectroscopy in general.

The suggested approach has important advantages:

1. Object definition and classification is much easier and more reliable on proper direct images with no interference from spectra. Photometry and astrometry are also more accurate.

2. Once an astrometric transformation from direct to spectroscopic image is established, one can *a priori* identify spectra that suffer from contamination from other objects (either 1st or other orders). In particular, the superposition of 0th and first orders from different sources can mimic emission line objects; this can be easily recognised with a direct image.

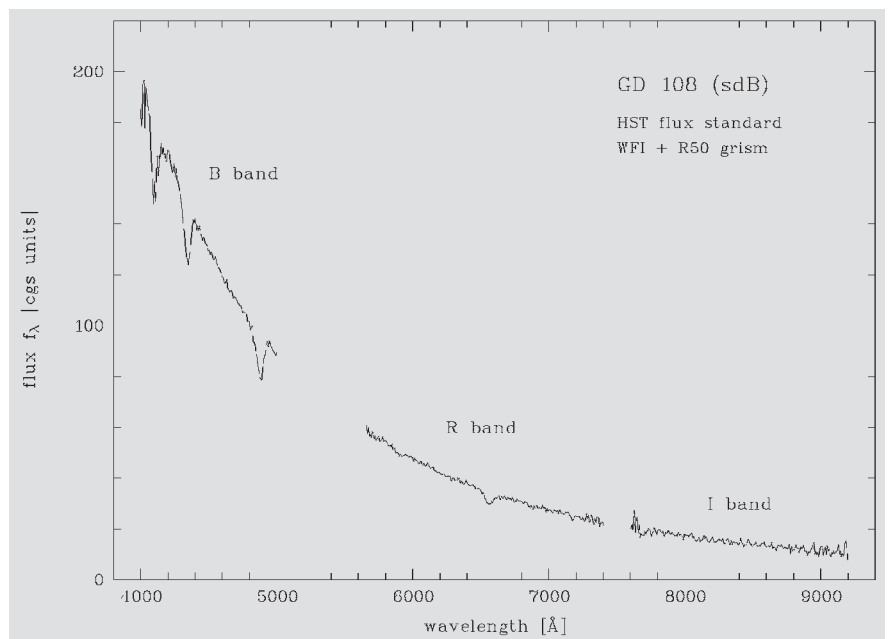


Figure 9: Spectra of the HST standard GD108.

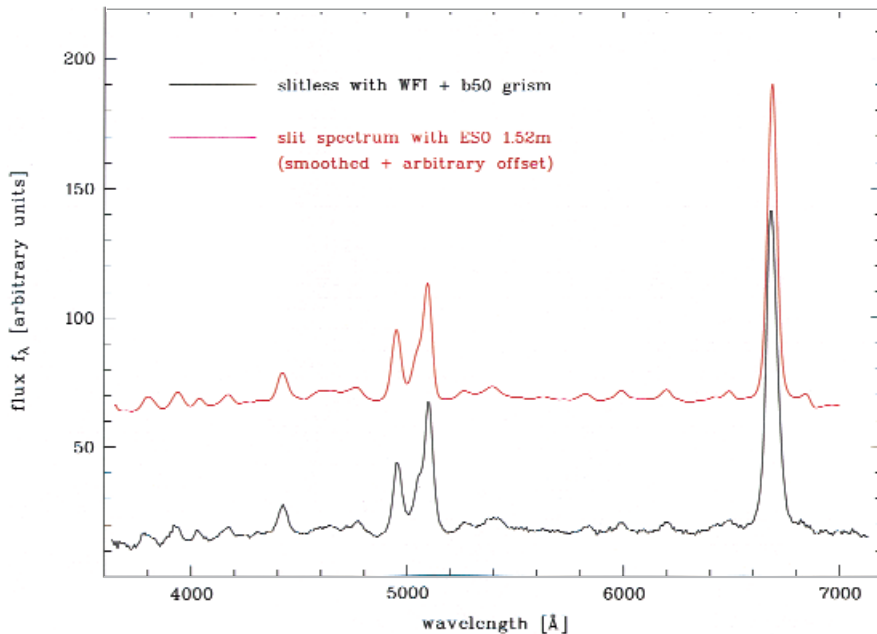


Figure 10: Spectra of the Seyfert 1 galaxy Mrk 1239. Lower spectrum in black: WFI slitless plus B50; upper spectrum in red: slit spectrum taken with ESO 1.52-m telescope.

3. Especially with certain medium-band filters, the 0th order can be so faint that it is barely detectable except for the brightest sources.

The direct image should be sufficiently deep as to allow the detection of all objects of interest. In certain applications, this may require a pretty long integration in the same filter band(s) selected for spectroscopy. Consider for example a search for continuum-free

emission-line objects with medium-band filters. Such objects are effectively point sources in the spectral images, so in order to reach similar depth in the direct image, almost comparable exposure times are needed.

#### Take flat fields in all filters

At the same time that the direct images are taken, one should obtain flat

fields in all the filters that will be used. The flattening of this kind of observations is an unsolved problem which will require further experimentation: the pixels exposed by the spectrum of an object each receive a different wavelength, monochromatic light, due to the object. When a flat field is obtained, those same pixels are illuminated by broad-band, or at best medium- or narrow-band light of the same spectral composition throughout.

#### Take rotated images in crowded fields

It is important to obtain images in at least two rotations if source crowding is important. Currently, the system allows only small rotations, less than 10 degrees, but this is more than enough to move zeroth and higher orders of neighbouring objects from the areas of interest.

#### References

- Bowen L. S., Vaughan A. H., 1973, "Non-objective" gratings, *PASP* **85**, 174.
- Hoag A. A., Schroeder D. J., 1970, "Non-objective" grating spectroscopy, *PASP* **85**, 174.
- Reimers D., Wisotzki L., 1997, *The Messenger* **88**, 14.
- Schneider D. P., Schmidt M., Gunn J. E., 1994, *AJ* **107**, 1245.
- Schneider D. P., Schmidt M., Gunn J. E., 1999, *AJ* **117**, 40.
- Wisotzki L., Christlieb N., Bade N., et al., 2000, *A&A* **358**, 77.

## VLT-Style Observing with the Wide Field Imager at the MPG/ESO 2.2-m Telescope at La Silla

C. URRUTIA<sup>1</sup>, T. PAZ<sup>1</sup>, E. ROBLEDO<sup>1</sup>, F. GUTIERREZ<sup>1</sup>, D. BAADE<sup>2</sup>, F. SELMAN<sup>1</sup>, F. SANCHEZ<sup>1</sup>, J. BREWER<sup>3</sup>, and M. SCODEGGIO<sup>4</sup>

<sup>1</sup>La Silla Observatory, ESO, Chile; <sup>2</sup>ESO, Garching; <sup>3</sup>University of British Columbia, Canada; <sup>4</sup>Istituto di Fisica Cosmica G. Occhialini, Italy

### 1. Introduction

The Wide Field Imager instrument of the MPG/ESO 2.2-m Telescope has been operating with the VLT-style Observing Software (OS) since the beginning of the year. Users can now prepare Observation Blocks in the same manner as for the VLT and other La Silla instruments. This uniformity of the user interface will make the system even more easy to use than before. This work is the result of the efforts of a large number of people: the sequencer scripts were written with extensive help from Paul Lesaux of the NTT team, and Emilio Barrios of the 3.6 team at La

Silla. Figure 1 shows the control room with the new system in place.

Testing and development was done during the normally scheduled idle times around full moon, having thus little impact on the functioning of the telescope. This was possible only because of the dedication of all persons involved. Special thanks to the Team's Telescope and Instrument Operators (TIOs), Roberto Castillo, Francisco Labraña, Mauricio Martinez, Jorge Araya, Jose Cortes, who had to suffer during the initial times before the system achieved stability. We would also like to gratefully acknowledge the patience of those users of the system

whose programmes were compromised by the initial teething problems.

### 2. Software Design

It was decided early on to keep the existing low-level subsystems and to build an interface layer from the existing Telescope Control System (TCS), Data Acquisition Integrated System (DAISY), which commands the instrument, and the WFI-specific installation of the FIERA control software, to the VLT compliant OS (for details on the TCS see *The Messenger*, No. 93, p.19, and No. 94, p.12). The resources available at the time did not permit the de-